Available online at www.sciencedirect.com

ScienceDirect

Ceramics International 40 (2014) 15531–15536

CERAMICS INTERNATIONAL

www.elsevier.com/locate/ceramint

High-temperature thermoelectric performance of $Ca_{0.96}Dy_{0.02}RE_{0.02}MnO_3$ ceramics (RE=Ho, Er, Tm)

Yuanhu Zhu*, Chunlei Wang, Wenbin Su, Jichao Li, Jian Liu, Yanling Du, Liangmo Mei

School of Physics, State Key Laboratory of Crystal Materials, Shandong University, Jinan 250100, China

Received 8 June 2014; received in revised form 26 June 2014; accepted 3 July 2014
Available online 11 July 2014

Abstract

Perovskite-type $Ca_{0.98}Dy_{0.02}MnO_3$ (CDM) and $Ca_{0.96}Dy_{0.02}RE_{0.02}MnO_3$ (RE=Ho, Er, Tm) (marked as CDM-Ho, CDM-Er, CDM-Tm) ceramics were prepared by solid state reaction. Their thermoelectric properties were evaluated between 300 K and 1000 K. All the samples are single phase with an orthorhombic structure. The introduction of second doping elements for RE=Ho, Er, Tm lead to a larger carrier concentration. As a result, the resistivity decreases from 36.1 mΩ cm for CDM to 12.4 mΩ cm for CDM-Ho at 973 K, while absolute Seebeck coefficient decreases from −300 μV/K for CDM to −196 μV/K for CDM-Tm. The highest power factor is obtained 350 μW/(K^2m) at 923 K for $Ca_{0.96}Dy_{0.02}Er_{0.02}MnO_3$ sample. And also the introduction of second element contributes to lower thermal conductivity. The highest figure of merit 0.23 is obtained for RE=Ho, Er samples at 973 K, representing an improvement of about 109% compared with $Ca_{0.98}Dy_{0.02}MnO_3$ sample.

Keywords: A. Sintering; C. Electrical properties; C. Thermal conductivity; Ceramics; Oxides

1. Introduction

Renewed attention has been paid on thermoelectric materials for their potential applications in converting heat to electricity and vice versa. The efficiency of thermoelectric materials is evaluated by the dimensionless thermoelectric figure of merit, $ZT=S^2\sigma T/\kappa$, where S, σ, T, and κ are the Seebeck coefficient, electrical conductivity, absolute temperature, and thermal conductivity, respectively [1,2].

On account of the low cost of raw materials and chemical stability, thermoelectric bulk oxides have been considered as promising candidate for power generation, especially at high temperature [3–5]. Since the discovery of Na_xCoO_2 by Terasaki et al. [6], modified cobaltates, such as $Ca_3Co_4O_9$ [7–9], $LaCoO_3$ [10,11], have been extensively studied as p-type legs for thermoelectric devices. However, as a counterpart, there are relatively few n-type oxide materials to be studied. Recently, $CaMnO_3$ has attracted attention as a prospective candidate of n-type thermoelectric oxides [12–14]. Thermoelectric performance of $CaMnO_3$ doped with rare-earth metals was first reported by Takizawa et al. [15] and Ohtaki et al. [16]. And following experiments, doping with some other trivalent elements, were carried out by Funahashi et al. [17] and Koumoto et al. [18]. They found that lanthanide elements doping at Ca site is an effective way to increase electrical conductivity and keep a moderate absolute Seebeck coefficient. And then Wang et al. [19–21] studied lanthanide elements substitution with a higher doping level of 10% and reported a large thermoelectric response of $CaMnO_3$ by doping Dy at Ca site. Whereafter, Liu et al. [22,23] found that a lower Dy doping level of 2% would also lead to a significant modification in $CaMnO_3$. On the basis of their study, we reported the thermoelectric performance of Dy/Bi dual doped $CaMnO_3$ and obtained a remarkable ZT=0.21 in $Ca_{0.96}Dy_{0.02}Bi_{0.02}MnO_3$ [24]. This result indicates that 2% dual doping at Ca site is effective in further improving thermoelectric performance of $CaMnO_3$. It was also reported the thermoelectric performance of $CaMnO_3$ improved by substituting Ho, Er etc. [15,19,25], indicating heavy lanthanide elements might be helpful in improving thermoelectric performance of $CaMnO_3$. Herein, in

*Corresponding author.

http://dx.doi.org/10.1016/j.ceramint.2014.07.028
0272-8842/

this paper we prepared $Ca_{0.96}Dy_{0.02}RE_{0.02}MnO_3$ with RE=Ho, Er, Tm (marked as CDM-Ho, CDM-Er, CDM-Tm), and also $Ca_{0.98}Dy_{0.02}MnO_3$ (CDM) as a comparison. Their thermoelectric properties were evaluated in temperature range between 300 K and 1000 K.

2. Experimental procedure

Solid state reaction method was used to synthesize samples of $Ca_{0.98}Dy_{0.02}MnO_3$ and $Ca_{0.96}Dy_{0.02}RE_{0.02}MnO_3$ ceramics, with RE=Ho, Er, Tm. The starting materials were $CaCO_3$ (99.8%), MnO_2 (99.9%), Dy_2O_3 (99.9%), Ho_2O_3 (99.99%), Er_2O_3 (99.99%) and Tm_2O_3 (99.99%) with the same provider of Sinopharm Group Co., Ltd. These raw materials were weighed in stoichiometric proportions and mixed by ball-milling in ethanol with zirconia balls for 12 h. After the wet mixtures dried, the powder was calcinated for 12 h at 1423 K and 12 h at 1523 K in ambient atmospheric condition with an intermediate grinding. The calcined powder was ball-milled for 12 h to obtain a fine powder. The products were pressed into pellets at 300 MPa, and sintered in air at 1573 K for 12 h. The sintered pellets were cut into rectangular columns with dimensions of 18 mm × 2.0 mm × 2.0 mm for measurement of thermoelectric properties.

X-ray powder diffraction (XRD) analysis was carried out using a Bruker AXS D8 ADVANCE diffractometer with Cu Kα radiation and scanning (a step width of 0.020°) over the angular range 20–70°. The density of the samples was measured by the Archimedes method. The electrical resistivity measurements were carried out with a standard four-probe in a helium atmosphere, and the Seebeck coefficient was measured simultaneously in the temperature range between 300 and 1100 K using LINSEIS LSR-3 equipment. Thermal conductivity values (κ) were calculated from the thermal diffusivity (λ), the specific heat capacity (C_p), and the density (d) by applying the following relationship:

$$\kappa = \lambda C_p d \quad (1)$$

The thermal diffusivity and specific heat capacity were measured with a laser flash apparatus (Netzsch LFA 457) and different thermal analyzers (Netzsch STA 449C), respectively. Then power factor, ZT and compatibility factor were calculated.

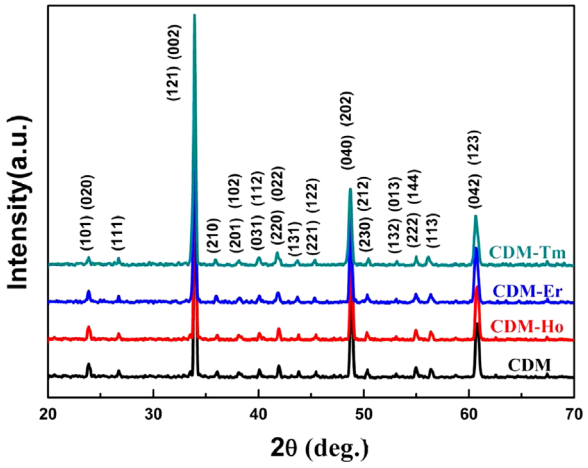

Fig. 1. Room temperature X-ray diffraction patterns for $Ca_{0.98}Dy_{0.02}MnO_3$ and $Ca_{0.96}Dy_{0.02}RE_{0.02}MnO_3$ (RE=Ho, Er, Tm).

3. Results and discussion

Fig. 1 shows X-ray diffraction (XRD) patterns at room temperature of CDM, CDM-Ho, CDM-Er, and CDM-Tm. All the diffraction peaks for the series of samples can be indexed based on an orthorhombic $CaMnO_3$ structure [24]. No second phase occurs, suggesting that the ions of Dy^{3+} and RE^{3+} have entered into the $CaMnO_3$ lattice. Lattice parameters are obtained from the X-ray data, theoretical density are calculated from the data and all listed in Table 1. As seen in Table 1, lattice parameters of dual doped samples are a little larger than that of CDM. However, we can get that the ionic radius of Ho^{3+} (1.015 Å), Er^{3+} (1.004 Å), and Tm^{3+} (0.994 Å) are all smaller than that of Ca^{2+} (1.12 Å) ions [26]. So the variation in lattice parameters may be mainly due to the increasing value of Mn^{3+}/Mn^{4+}, because of the different size in the ionic radii between Mn^{3+} (0.645 Å) and Mn^{4+} (0.530 Å) [26]. This phenomenon has also been reported by us in Dy/Yb dual-doping $CaMnO_3$ [5]. Experimental densities are 4.561 g/cm^3, 4.590 g/cm^3, 4.568 g/cm^3 and 4.629 g/cm^3 for samples of CDM, CDM-Ho, CDM-Er, and CDM-Tm, respectively. For dual doping samples, the measured density increases with the increase of atomic number, mainly due to the contribution from the heavier mass of Ho, Er, and Tm elements. The relative densities, defined as the experimental density over the theoretical density, are all 96.0–97.2%, which means the samples are of good compactness.

The temperature dependence of resistivity for CDM, CDM-Ho, CDM-Er, and CDM-Tm is shown in Fig. 2. All samples exhibit metal-like behavior, i.e., the resistivity decreases with increasing temperature ($d\rho/dT > 0$) which is observed in the entire temperature range. Similar tendency was also reported in other doped $CaMnO_3$ samples [20–24]. At high temperature

Table 1
Lattice parameters, densities of $Ca_{0.98}Dy_{0.02}MnO_3$ and $Ca_{0.96}Dy_{0.02}Re_{0.02}MnO_3$ (Re=Ho, Er, Tm).

Samples	a (Å)	b (Å)	c (Å)	Theoretical density (g/cm^3)	Experimental density (g/cm^3)	Relative density (%)
CDM	5.272(6)	7.466(2)	5.270(4)	4.701	4.561	97.0
CDM-Ho	5.285(3)	7.481(2)	5.280(1)	4.752	4.590	96.6
CDM-Er	5.289(6)	7.490(3)	5.281(5)	4.758	4.568	96.0
CDM-Tm	5.291(5)	7.494(2)	5.286(9)	4.763	4.629	97.2

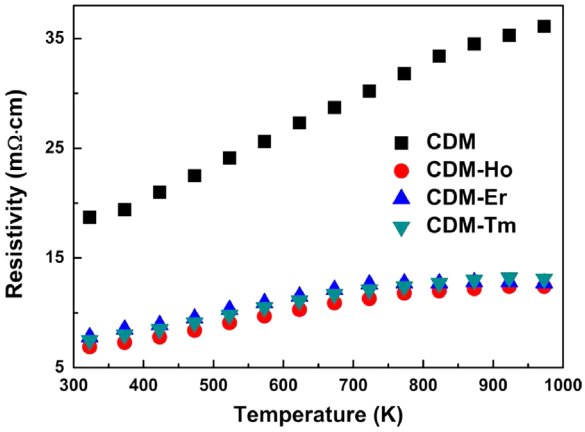

Fig. 2. Temperature dependence of electrical resistivity for $Ca_{0.98}Dy_{0.02}MnO_3$ and $Ca_{0.96}Dy_{0.02}RE_{0.02}MnO_3$ (RE=Ho, Er, Tm).

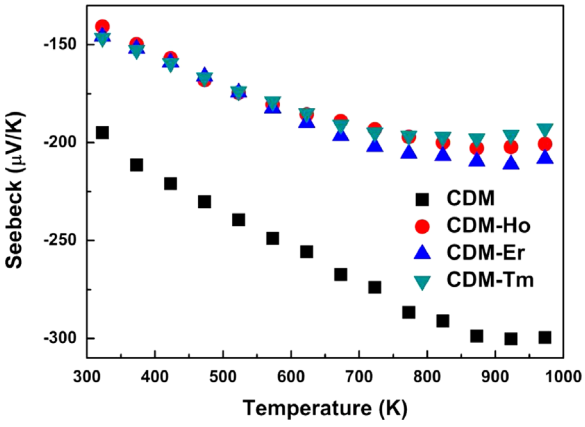

Fig. 3. Temperature dependence of the Seebeck coefficient for $Ca_{0.98}Dy_{0.02}MnO_3$ and $Ca_{0.96}Dy_{0.02}RE_{0.02}MnO_3$ (RE=Ho, Er, Tm).

973 K, the values of resistivity are obtained 36.1 mΩ cm, 12.4 mΩ cm, 12.7 mΩ cm and 13.2 mΩ cm, for samples of CDM, CDM-Ho, CDM-Er, and CDM-Tm, respectively. It can be seen that the resistivity decreases remarkably as the second element introduced into CDM. And no visible difference is observed among the three dual doped samples. Since resistivity depends on the carrier concentration and the mobility, the similar trend of resistivity among the three dual doping samples may imply a similarity in the carrier concentration and mobility.

Temperature dependence of Seebeck coefficients for CDM, CDM-Ho, CDM-Er, and CDM-Tm ceramics is shown in Fig. 3. In the whole temperature range between 300 K and 1000 K, the Seebeck coefficients are all negative, indicating an n-type electrical conduction behavior. The sample of CDM has a relatively large absolute Seebeck coefficient, being about −300 μV/K at 973 K. As the second additional element introduced into CDM, the dual doped samples show relatively smaller absolute Seebeck coefficients. This phenomenon is attributed to the increase of carrier concentration. Also it is seen that all dual doped samples show a similar trend in the values of Seebeck coefficients. As Seebeck coefficient depends on the nature and concentration of the charge carrier, this implies that the three dual doping samples may share similar carrier concentration, which is also confirmed by the similarity in their resistivity. From previous dual doping reports [17,24], we can conclude that the second element introduces larger carrier concentration. When Ho^{3+}, Er^{3+} and Tm^{3+} substitute Ca^{2+} in CDM, they are expected to behave as donor ions. This leads to the increase of carrier concentration, and now we can say that the increases of carrier concentration are almost the same for CDM-Ho, CDM-Er and CDM-Tm. The Seebeck coefficient of CDM sample is nearly linear function of temperature from 300 K to 900 K, and for dual doped samples the linear curves are only observed from 300 K to 750 K. The linear relationship of Seebeck coefficients with temperature, in accord with the behavior reported before [21,24], implies a behavior of the electron conduction. Therefore, the metal-like resistivity and linear temperature dependence of Seebeck coefficient allow us to use the modified expression for Seebeck coefficient of single-band metal, and thus the Seebeck coefficient S can be expressed as [27]

$$S = -\frac{\pi^2 k_B^2 T}{3|e|}\left(\frac{N(E)}{n} + A\right)_{E=E_F} \quad (2)$$

where k_B, e, $N(E)$, n, and A, are Boltzmann constant, electron charge, density of states, carrier concentration, and material constant, respectively. The least square fit of the experimental data in Fig. 3 with Eq. (2) yields the slopes of the S–T curve, which are 0.184, 0.132, 0.144, 0.125 for CDM, CDM-Ho, CDM-Er, and CDM-Tm, respectively. It can be seen that these values of slopes for the three dual doped samples are similar with each other. As we confirmed that the carrier concentration for three dual doped samples were similar and the slopes are determined by the values of $N(E)/n$, we could get a conclusion that the density of states around Fermi level for three dual doped samples are almost same. Also, this conclusion still needs the recognition from theoretical calculation.

However, at high temperatures, values of Seebeck coffi-cients become saturated and temperature-independent for all samples. This indicates that there is a narrow conducting band around the Fermi energy E_F at high temperature, according to the Heikes and Ure's theory [28]. Their study shows us that the Seebeck coefficient of a narrow band is predicted to saturate and become temperature-independent when temperature is high enough that k_BT is larger than the width of the band [28]. The saturating temperature T_s is proportional to the width of the narrow band [28], which is around 900 K for CDM and for dual doped samples is around 750 K. Therefore, the conducting band becomes narrower when the second elements are doped into CDM. This phenomenon can also be found in previous reports by Wang et al. [19–21] and our group [24].

Power factor (PF) is calculated from Seebeck coefficient and electrical resistivity as S^2/ρ. The temperature dependence of power factor is shown in Fig. 4. It can be seen that power factors do not change with temperature dramatically in the temperature range between 300 K and 1000 K. Obviously, the power factors increase with the second element introduced into CDM. The highest values of PF are 257 μW/(K^2 m), 335 μW/(K^2 m), 350 μW/(K^2 m), 314 μW/(K^2 m) for CDM, CDM-Ho,

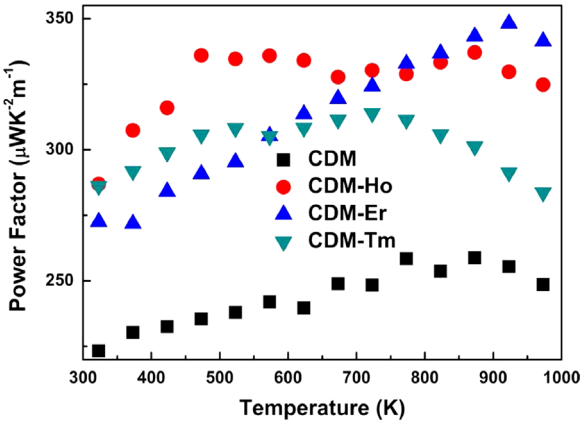

Fig. 4. Temperature dependence of the power factor for $Ca_{0.98}Dy_{0.02}MnO_3$ and $Ca_{0.96}Dy_{0.02}RE_{0.02}MnO_3$ (RE=Ho, Er, Tm).

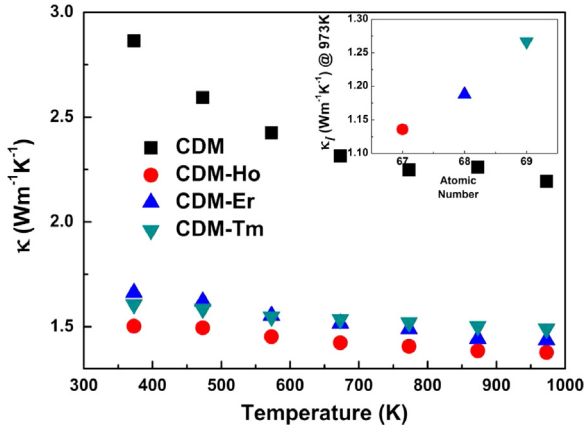

Fig. 5. Temperature dependence of thermal conductivity for $Ca_{0.98}Dy_{0.02}MnO_3$ and $Ca_{0.96}Dy_{0.02}RE_{0.02}MnO_3$ (RE=Ho, Er, Tm), and inset plots lattice thermal conductivity at 973 K for $Ca_{0.96}Dy_{0.02}RE_{0.02}MnO_3$ (RE=Ho, Er, Tm).

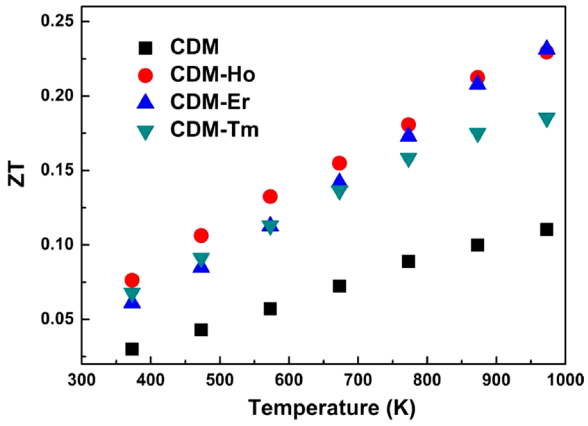

Fig. 6. Temperature dependence of dimensionless figure-of-merit ZT for $Ca_{0.98}Dy_{0.02}MnO_3$ and $Ca_{0.96}Dy_{0.02}RE_{0.02}MnO_3$ (RE=Ho, Er, Tm).

CDM-Er, and CDM-Tm, respectively. It can be seen that CDM-Er sample exhibits the highest value of power factor at high temperature. This is related with the effectively decreasing of electrical resistivity while maintaining a reasonable value of Seebeck coefficient by dual doping of Dy and Er.

Temperature dependence of thermal conductivity (κ) between 300 K and 1000 K is shown in Fig. 5. As all samples are with high relative density 96.0–97.2% shown in Table 1, the ratio of hole for all samples is relatively small, and the difference of ratio of hole for each sample is not distinct. Therefore, the effect of porosity on thermal conductivity in different samples can be ignored. The lowest value of thermal conductivity for CDM is 2.20 W/m K at 973 K. And for CDM-Ho, CDM-Er, and CDM-Tm, the lowest values are obtained 1.38 W/m K, 1.44 W/m K, 1.50 W/m K, respectively, at 973 K. The low values indicate that they are all oxide thermoelectric materials with low thermal conductivity. It is easily seen that in whole temperature range the thermal conductivity for dual doping samples are lower than that of CDM. This result leads to the fact that dual doping is more effective in reducing thermal conductivity on $CaMnO_3$ than single doping. The difference of the thermal conductivity for different dual doping samples is small, only 8–12%. This result indicates that the effects in reducing thermal conductivity for different second elements are almost the same. It is well known that the thermal conductivity (κ) could be expressed by the sum total of the lattice thermal conductivity (κ_l) and the electronic thermal conductivity (κ_e). Usually, electronic thermal conductivity is determined by the Wiedemann–Franz law (3) as below

$$\kappa_e = LT\sigma \tag{3}$$

where $L=2.45\times10^{-8}\,\mathrm{W\,\Omega\,K^{-2}}$ is the Lorenz number, σ is the electrical conductivity, and T is the absolute temperature. The lattice thermal conductivity at 973 K for different dual doped samples is obtained by subtracting the electronic thermal conductivity from the thermal conductivity, shown in Fig. 5 (inset). It is easy to be observed that the lattice thermal conductivity increases with the atomic number of second doping element, from Ho (No. 67) to Tm (No. 69). It suggests that, for the second doping elements, the closer it gets to the atomic number of Dy (No. 66), the lower sample's lattice thermal conductivity becomes. As seen in Fig. 5, the value of lattice thermal conductivity is close to that of thermal conductivity. This indicates that the thermal conductivity mainly comes from the lattice thermal conductivity, which can be qualitatively supposed that the lattice component dominates thermal conductivity. According to the study of Wang et al. [19], the low lattice thermal conductivity for dual doping samples is mainly due to the variation in lattice vibration of the system strongly caused by RE^{3+} doping. The effect of RE^{3+} doping on the lattice vibration arises from two main factors. One is that the weight of RE^{3+} is much higher than that of Ca^{2+}. So the RE^{3+} ions can vibrate independently from the other ions, which would cause large local vibrations [19]. As a result, the average free path of phonons will be shortened, and thus lattice thermal conductivity will be markedly suppressed. The other factor is the crystallographic distortion caused by the change in ionic radius, which would lead to further reduction in lattice thermal conductivity [16].

Temperature dependence of dimensionless figure-of-merit ZT is shown in Fig. 6. The values of ZT for all of the samples increase with temperature in the whole temperature range. The single doped sample CDM shows similar ZT values to the previous report by Liu et al. [22,23] The highest value for CDM sample is about 0.11 at 973 K, which is about twice than that of un-doped $CaMnO_3$ according to Ref. [24]. And the ZT values of CDM-Ho, CDM-Er, and CDM-Tm, are all higher than that of CDM. The highest ZT value reaches 0.23 at temperature around 973 K for both CDM-Ho and CDM-Er, which represents 109% improvement compared with single dysprosium-doped sample CDM. This value is comparable to p-type oxide $Ca_3Co_4O_9$ with ZT $\sim$0.1–0.3, which has been widely studied as high-temperature thermoelectric material [29–32]. And it confirms that these manganites could be good candidates as n-type materials for high temperature thermoelectric application.

4. Conclusion

Perovskite-type $Ca_{0.98}Dy_{0.02}MnO_3$ and $Ca_{0.96}Dy_{0.02}RE_{0.02}MnO_3$ (RE=Ho, Er, Tm) ceramics have been obtained by solid state reaction method. Thermoelectric properties are investigated in temperature range between 300 K and 1000 K. Dual doping is found very effective to reduce the electrical resistivity, and keep a moderate absolute Seebeck coefficient. The introduction of second element leads to a remarked lower thermal conductivity. The highest ZT=0.23 at 973 K is obtained in both $Ca_{0.96}Dy_{0.02}Ho_{0.02}MnO_3$ and $Ca_{0.96}Dy_{0.02}Er_{0.02}MnO_3$ and it is about 109% improved compared with $Ca_{0.98}Dy_{0.02}MnO_3$ sample at the same temperature. This suggests that doping with the second element is very effective to improve the thermoelectric performance of $Ca_{0.98}Dy_{0.02}MnO_3$. Besides, in order to improve further the thermoelectric properties of $CaMnO_3$ system, other kinds of trivalent element doping on $Ca_{0.98}Dy_{0.02}MnO_3$ need further investigation.

Acknowledgments

The work is financially supported by the National Basic Research Program of China under Grant no. 2013CB632506, the Natural Science Foundation of China (11374186, 51231007 and 51202132), and Independent Innovation Foundation of Shandong University, IIFSDU.

References

[1] T.M. Tritt, Holey and unholey semiconductors, Science 283 (1999) 804–805.
[2] J.P. Heremans, V. Jovovic, E.S. Toberer, A. Saramat, K. Kurosaki, A. Charoenphakdee, S. Yamanaka, G.J. Snyder, Enhancement of thermoelectric efficiency in PbTe by distortion of the electronic density of states, Science 321 (2008) 554–557.
[3] L. Bocher, M.H. Aguirre, D. Logvinovich, A. Shkabko, R. Robert, M. Trottmann, A. Weidenkaff, $CaMn_{1-x}Nb_xO_3$ ($x \le 0.08$) perovskite-type phases as promising new high-temperature n-type thermoelectric materials, Inorg. Chem. 47 (2008) 8077–8085.
[4] M. Rosic, M. Logar, J. Zagorac, A. Devecerski, A. Egelja, V. Kusigerski, V. Spasojevic, B. Matovic, Investigation of the structure and the magnetic behavior of nanostructure $Ca_{1-x}Gd_xMnO_3$ (x=0.05; 0.1; 0.15; 0.2) obtained by modified glycine nitrate procedure, Ceram. Int. 39 (2013) 1853–1861.
[5] H.C. Wanga, C.L. Wang, Synthesis of Dy doped $Yb_{0.1}Ca_{0.9}MnO_3$ ceramics with a high relative density and their thermoelectric properties, Mater. Res. Bull. 47 (2012) 2252–2256.
[6] I. Terasaki, Y. Sasago, K. Uchinokura, Large thermoelectric power in $NaCo_2O_4$ single crystals, Phys. Rev. B 56 (1997) 12685–12687.
[7] Y.H. Lin, J.L. Lan, Z.J. Shen, Y.H. Liu, C.W. Nan, J.F. Li, High-temperature electrical transport behaviors in textured $Ca_3Co_4O_9$-based polycrystalline ceramics, Appl. Phys. Lett. 94 (2009) 072107.
[8] G. Constantinescu, M.A. Madre, Sh. Rasekh, M.A. Torres, J.C. Diez, A. Sotelo, Effect of Ga addition on Ca-deficient $Ca_3Co_4O_y$ thermoelectric materials, Ceram. Int. 40 (4) (2014) 6255–6260.
[9] A. Bhaskar, Y.-C. Huang, C.-J. Liu, Improvement on the low-temperature thermoelectric characteristics of $Ca_{3-x}Yb_xCo_4O_{9+\delta}$ ($0 \le x \le 0.10$), Ceram. Int. 40 (4) (2014) 5937–5943.
[10] J. Androulakis, P. Migiakis, J. Giapintzakis, $La_{0.95}Sr_{0.05}CoO_3$: an efficient room-temperature thermoelectric oxide, Appl. Phys. Lett. 84 (2004) 1099–1101.
[11] F. Li, J.-F. Li, Effect of Ni substitution on electrical and thermoelectric properties of $LaCoO_3$ ceramics, Ceram. Int. 37 (7) (2011) 105–110.
[12] F.P. Zhang, X. Zhang, Q.M. Lu, J.X. Zhang, Y.Q. Liu, Electronic structure and thermal properties of doped $CaMnO_3$ systems, J. Alloy. Compd. 509 (2011) 4171–4175.
[13] J.L. Lan, Y.-H. Lin, H. Fang, A. Mei, C.-W. Nan, Y. Liu, S.L. Xu, M. Peters, High-temperature thermoelectric behaviors of fine-grained Gd-doped $CaMnO_3$ ceramics, J. Am. Ceram. Soc. 93 (8) (2010) 2121–2124.
[14] H. Muguerra, B. Rivas-Murias, M. Traianidis, C. Marchal, Ph. Vanderbemden, B. Vertruyen, C. Henrist, R. Cloots, Thermoelectric properties of n-type $Ca_{1-x}Dy_xMn_{1-y}NbyO_{3-1}$ compounds (x=0, 0.02, 0.1 and y=0, 0.02) prepared by spray-drying method, J. Alloy. Compd 509 (2011) 7710–7716.
[15] T. Kobayashi, H. Takizawa, T. Endo, T. Sato, M. Shimada, H. Taguchi, M. Nagao, Metal-insulator transition and thermoelectric properties in the system $(R_{1-x},Ca_x)MnO_{3-\delta}$ (R: Tb, Ho, Y), J. Solid State Chem. 92 (1991) 116–129.
[16] M. Ohtaki, H. Koga, T. Tokunaga, K. Eguchi, H. Arai, Electrical transport properties and high-temperature thermoelectric performance of $(Ca_{0.9}M_{0.1})MnO_3$ (M=Y, La, Ce, Sm, In, Sn, Sb, Pb, Bi), J. Solid State Chem. 120 (1995) 105–111.
[17] A. Kosuga, Y. Isse, Y.F. Wang, K. Koumoto, R. Funahashi, High-temperature thermoelectric properties of $Ca_{0.9-x}Sr_xYb_{0.1}MnO_{3-\delta}$ ($0 \le x \le 0.2$), J. Appl. Phys. 105 (2009) 093717.
[18] D. Flahaut, T. Mihara, R. Funahashi, N. Nabeshima, K. Lee, H. Ohta, K. Koumoto, Thermoelectrical properties of A-site substituted $Ca_{1-x}Re_xMnO_3$ system, J. Appl. Phys. 100 (2006) 084911.
[19] Y. Wang, Y. Sui, W.H. Su, High temperature thermoelectric characteristics of $Ca_{0.9}R_{0.1}MnO_3$ (R=La,Pr,…,Yb), J. Appl. Phys. 104 (2008) 93703.
[20] Y. Wang, Y. Sui, H.J. Fan, X.J. Wang, Y.T. Su, W.H. Su, X.Y. Liu, High temperature thermoelectric response of electron-doped $CaMnO_3$, Chem. Mater. 21 (2009) 4653–4660.
[21] Y. Wang, Y. Sui, X.J. Wang, W.H. Su, Enhancement of thermoelectric efficiency in $(Ca,Dy)MnO_3$–$(Ca,Yb)MnO_3$ solid solutions, Appl. Phys. Lett. 97 (2010) 052109.
[22] C.-J. Liu, A. Bhaskar, J.J. Yuan, High-temperature transport properties of $Ca_{0.98}RE_{0.02}MnO_{3-\delta}$ (RE=Sm, Gd, and Dy), Appl. Phys. Lett. 98 (2011) 214101.
[23] A. Bhaskar, C.-J. Liu, J.J. Yuan, Thermoelectric and magnetic properties of $Ca_{0.98}RE_{0.02}MnO_{3-\delta}$ (RE=Sm, Gd, and Dy), J. Electron. Mater. 41 (9) (2012) 2338–2344.
[24] Y.H. Zhu, C.L. Wang, H.C. Wang, W.B. Su, J. Liu, J.C. Li, Influence of Dy/Bi dual doping on thermoelectric performance of $CaMnO_3$ ceramics, Mater. Chem. Phys. 144 (2014) 385–389.
[25] Y.J. Li, S. Hao, X. Xia, J.L. Xu, X. Du, S.Y. Fang, X.W. Meng, Preparation, structure, and electrical properties of $Ca_{1-x}Er_xMnO_3$ powders, J. Electron. Mater. 42 (4) (2013) 745.

[26] R.D. Shannon, Revised effective ionic radii and systematic studies of interatomic distances in halides and chalcogenides, Acta Crystallogr. A32 (1976) 751–767.
[27] J. Hejtmanek, Z. Jirak, M. Marysko, Interplay between transport, magnetic, and ordering phenomena in $Sm_{1-x}Ca_xMnO_3$, Phys. Rev. B 60 (1999) 14057–14065.
[28] R.R. Heikes, R.W. Ure, Thermoelectricity, Interscience, New York, 1961.
[29] I. Matsubara, R. Funahashi, T. Takeuchi, S. Sodeoka, T. Shimizu, K. Ueno, Fabrication of an all-oxide thermoelectric power generator, Appl. Phys. Lett. 78 (2001) 3627–3629.
[30] C.-H. Lim, S.-M. Choi, W.-S. Seo, H.-H. Park, Power-generation test for oxide-based thermoelectric modules using p-type $Ca_3Co_4O_9$ and n-Type $Ca_{0.9}Nd_{0.1}MnO_3$ legs, J. Electron. Mater. 41 (6) (2012) 1247–1255.
[31] D. Kenfaui, M. Gomina, D. Chateigner, J.G. Noudem, Mechanical properties of $Ca_3Co_4O_9$ bulk oxides intended to be used in thermoelectric generators, Ceram. Int. 40 (7B) (2014) 10237–10246.
[32] L. Han, Y. Jiang, S.Y. Li, H.M. Su, X.Z. Lan, K.X. Qin, T.T. Han, H. H. Zhong, L. Chen, D.B. Yu, High temperature thermoelectric properties and energy transfer devices of $Ca_3Co_{4-x}Ag_xO_9$ and $Ca_{1-y}Sm_yMnO_3$, J. Alloy. Compd. 509 (2011) 8970–8977.